ROYAL SOCIETY OPEN SCIENCE

royalsocietypublishing.org/journal/rsos

Research

Cite this article: Luo L, Wu X, Li Z, Zhou Y, Chen T, Fan M, Zhao W. 2019 Synthesis of activated carbon from biowaste of fir bark for methylene blue removal. *R. Soc. open sci.* **6**: 190523.
http://dx.doi.org/10.1098/rsos.190523

Received: 24 May 2019
Accepted: 5 August 2019

Subject Category:
Chemistry

Subject Areas:
environmental chemistry

Keywords:
fir bark, activated carbon, adsorption, methylene blue

Author for correspondence:
Weigang Zhao
e-mail: weigang-zhao@hotmail.com

This article has been edited by the Royal Society of Chemistry, including the commissioning, peer review process and editorial aspects up to the point of acceptance.

THE ROYAL SOCIETY PUBLISHING

Synthesis of activated carbon from biowaste of fir bark for methylene blue removal

Lu Luo[1], Xi Wu[1], Zeliang Li[1], Yalan Zhou[1], Tingting Chen[1], Mizi Fan[1,2] and Weigang Zhao[1]

[1]College of Material Engineering, Fujian Agriculture and Forestry University, 63 Xiyuangong Road, Fuzhou 350002, People's Republic of China
[2]College of Engineering Design and Physical Sciences, Brunel University, Uxbridge UB8 3PH, UK

WZ, 0000-0003-1804-6552

Activated carbon (AC) was successfully prepared from low-cost forestry fir bark (FB) waste using KOH activation method. Morphology and texture properties of ACFB were studied by scanning and high-resolution transmission electron microscopies (SEM and HRTEM), respectively. The resulting fir bark-based activated carbon (ACFB) demonstrated high surface area (1552 $m^2 g^{-1}$) and pore volume (0.84 $cm^3 g^{-1}$), both of which reflect excellent potential adsorption properties of ACFB towards methylene blue (MB). The effect of various factors, such as pH, initial concentration, adsorbent content as well as adsorption duration, was studied individually. Adsorption isotherms of MB were fitted using all three nonlinear models (Freundlich, Langmuir and Tempkin). The best fitting of MB adsorption results was obtained using Freundlich and Temkin. Experimental results showed that kinetics of MB adsorption by our ACFB adsorbent followed pseudo-second-order model. The maximum adsorption capacity obtained was 330 mg g^{-1}, which indicated that FB is an excellent raw material for low-cost production of AC suitable for cationic dye removal.

1. Introduction

As urbanization and industrialization advance, the environmental problem has become increasingly prominent, especially the pollution of water resources, which seriously affects water quality [1]. Among the pollutants, synthetic dyes (i.e. methylene blue (MB)) have drawn much attention because of their wide application in dyeing, textiles, printing, leather as well as in the coating industries, which causes water contamination [2,3]. Meanwhile, coloured dye wastewater is complex in nature, most of which is toxic, mutagenic and carcinogenic to aquatic organisms, causing some health problems [4,5]. MB is a very commonly used

synthetic dye (in wood, silk, leather and cotton processing) and, as a result, is often found in industrial wastewater. It belongs to the group of cationic dyes. The ingestion of water with MB into the human body can lead to health problems such as shock, diarrhoea, jaundice, etc. [5,6].

Based on the problems, several technologies, including flotation [7], aerobic and anaerobic treatment [8], micro-and ultra-filtration [9], ion exchange [10], microbial electrochemical technologies [11], oxidation [12,13] and adsorption, have been employed for wastewater treatment [14–18]. Among these methods, adsorption has received extensive attention since it is easier, cheaper, more efficient and economical than others. Thus, different adsorbents have been developed and applied to neutralize dyes and other organics in wastewater. Nguyyen & Juang [19] prepared graphene oxide/titanate nanotube compound and when applied for adsorption of MB, the adsorption capacity was low, only 26 mg g^{-1}. Yang *et al*. [20] synthesized the graphite oxide using a kitchen microwave oven and the adsorption capacity of MB was 170 mg g^{-1}. Dehghani *et al*. [21] used a new composite made up of shrimp waste chitosan and zeolite as adsorbent to remove MB, and the adsorption capacity was 24.5 mg g^{-1}. Fu *et al*. [22] synthesized polydopamine (PDA) microspheres by oxidative polymerization method and used them as an adsorbent for the removal of MB, with the adsorption capacity reaching 90.7 mg g^{-1}. Auta & Hameed [23] reported that Chitosan–clay composite was prepared and applied to remove MB, and the adsorption capacity was 142 mg g^{-1}. Therefore, it is necessary to develop an efficient and environmentally-friendly adsorbent.

Activated carbon (AC) is one of the best adsorbents which is widely used because of its large surface area, excellent porosity, low density as well as high adsorption capacity towards various organic compounds [1,24–26]. ACs can be obtained from various agricultural waste- and by-products, which have received significant attention as they are low-cost, renewable and environmentally friendly [25,27]. Recently, several types of ACs were obtained using bamboo [28], palm shells [29], coconut shell [30,31], rich husk [32], sawdust [33], apricot stones [34], seeds [27], etc. as raw materials. The fir tree is one of the fastest-growing trees to be planted in large numbers throughout the world. As a common forestry waste, the tree bark is a low added value product, which is often burned as a fuel or treated as waste material [33]. In the course of fir tree use, a large amount of fir bark (FB) is produced, which causes gaseous pollution during burning.

Therefore, this work is focused on the preparation of AC from FB (ACFB) using the KOH activation method. As mentioned, fir tree bark is a cost-effective and high-quantity by-product, which makes it a very promising raw material for preparing low-cost activated biocarbons. To evaluate the properties of this ACFB, we used its dye adsorption capacity towards MB as a performance criterion. When not used as a fuel or treated as waste material, the value-added applications of fir tree bark have important implications for both society and the environment. The morphology texture and pore structure of ACFB were characterized using SEM and BET analyses, respectively. MB was selected to study the adsorption capacity. The effect of contact time, adsorbent dosage, initial concentration and pH on adsorption characteristics of ACFB was studied. The fitting of adsorption isotherms and kinetics were also investigated. The results suggest the as-prepared porous carbon material from fir tree bark has great potential for MB adsorption, which is comparable or better than the samples reported in the open literature.

2. Material and methods

2.1. Reagents and materials

Chinese fir (*Cunninghamia lanceolata*) bark as raw material was sourced from a commercial plantation in Fujian province (China). KOH pellets and HCl solution (approx. 36.5%), used as received, were of analytical grade and acquired from Tianjin Fuchen Chemical Reagents Factory (Tianjin, China). We used deionized water with 18.25 MΩ cm resistance.

2.2. Activated carbon synthesis

For the synthesis of activated carbon (ACFB), Chinese fir was washed several times with tap water until the waste water became clear. It was dried at 103°C for 24 h, after which the bark was milled and sieved through a 10 mesh sieve to obtain powder around approximately 2 mm in size.

The synthesis procedure of AC was adapted from our earlier work as follows [35]: first, crushed FB was carbonized at 450°C (from room temperature at 5°C min^{-1} rate) under constant N_2 flow of 500 ml min^{-1}. After 1 h held at 450°, the samples were slowly cooled at room temperature. The resulting product was a carbonaceous precursor, which was then mixed with KOH pellets. The mixture was placed into a nickel crucible and then into a tube furnace, which was slowly heated (at 3°C min^{-1}) to 700°C under a constant

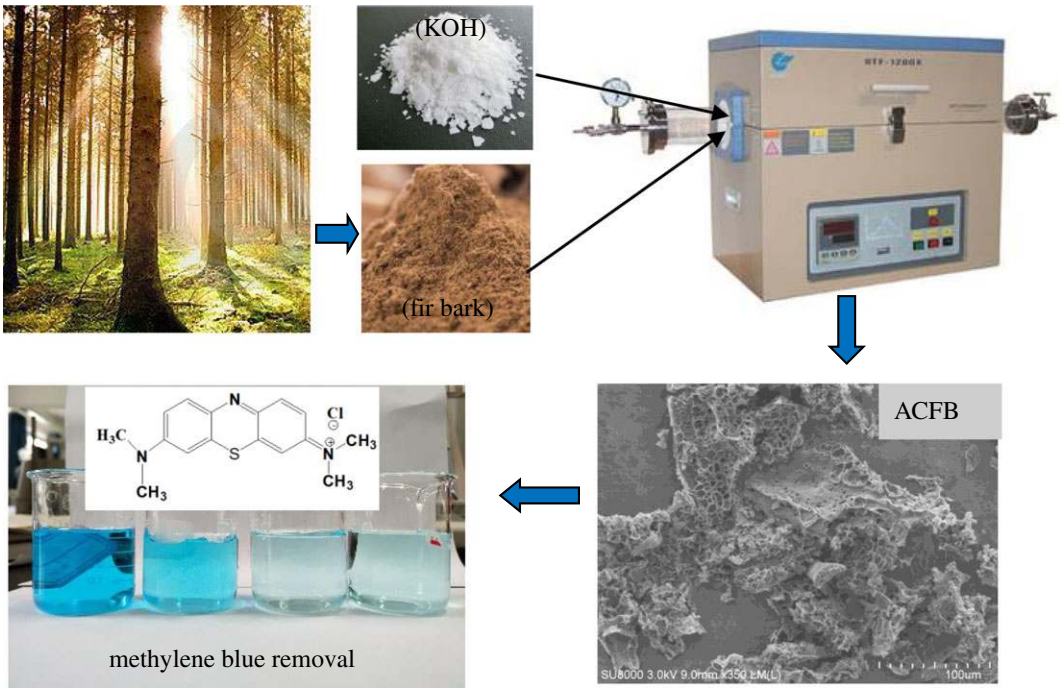

Figure 1. Schematic procedure of the complete synthesis route of the porous carbons from FB for MB removal.

N_2 flow (500 ml min^{-1}). After 2 h at 700°C, the samples were allowed to cool down inside the tube furnace still under nitrogen flow. The resulting AC samples were rinsed with 1 M HCl and then washed with hot water in Soxhlet for 48 h until the pH of water was stable, after which the products were dried for 24 h at 103°C. The resulting product was very pure AC. Because it was prepared from FB, it was named ACFB (figure 1).

2.3. Characterization methods

Specific surface area as well as pore volume and sizes of ACFB were obtained by Micromeritics ASAP 2020 automatic apparatus using nitrogen adsorption/desorption isotherms at −196°C. ACFB was degassed at 250°C under vacuum overnight. The average micropore diameters (L_0) and pore size distributions (PSD) were calculated using density functional theory (DFT). The surface morphology and pore texture of ACFB were characterized using scanning transmission electron microscopy (STEM; FEG SEM Hitachi S3400, Chiyoda-ku, Tokyo, Japan) as well as high-resolution transmission electronic microscopy (HRTEM; JEM-2100, JEOL, Tokyo, Japan) at 200 kV accelerating voltage.

2.4. Adsorption of dyes on methylene blue

Adsorption experiments were performed using the batch adsorption method to determine the influence of pH (in the 3–11 range), initial adsorbent content (in the 20–80 mg l^{-1} range), ACFB dose (1–50 mg) and adsorption duration (5–180 min) on the adsorption result. For each experiment, a certain amount of ACFB was placed into a 250 ml conical flask containing 100 ml of MB of a specific concentration and at certain pH. The mixture was stirred in an orbital shaker at 30°C at 150 rpm over a specific time. Remaining MB content was measured by UV–vis UV-6300, MAPADA spectrophotometer at 664 nm maximum wavelength.

The percentage of MB adsorbed was determined based on the following formula:

$$\text{Removal}\ \ (\%) = \frac{C_0 - C_e}{C_0} \times 100. \tag{2.1}$$

The maximum MB uptake q_e (in mg g^{-1}) was calculated as shown below

$$q_e = \frac{C_0 - C_e}{W} \times V, \tag{2.2}$$

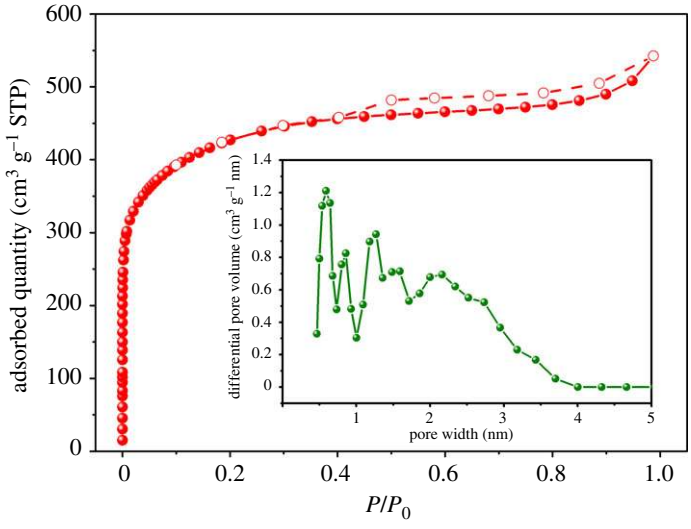

Figure 2. Nitrogen sorption (filled symbols)/desorption (empty symbols) isotherms and PSD (inset) for ACFB.

where C_0 and C_e are initial and final MB concentrations in mg l^{-1}, respectively; W is the amount of ACFB (in g) and V is the volume of MB solution (in l).

3. Results and discussion

3.1. Characterization of carbon material

N_2 nitrogen adsorption/desorption isotherms at −196°C as well as PSDs of ACFB are shown in figure 2. The nitrogen adsorption amount increased obviously at P/P_0 below 0.05, which indicated the mainly microporosity of ACFB [35,36]. ACFB isotherms in the 0.4–0.99 P/P_0 range belong to type I isotherm with H4 hysteresis according to the IUPAC classification. Such isotherms are typical for materials with a wide pore distribution, including mesopores, which were present in our ACFB [35,37]. PSD obtained using DFT calculations also showed a wide range: from 0.5 to 4 nm (figure 2 (inset)), which confirmed the results above. BET analysis showed that the surface area of ACFB was as high as 1552 m^2 g^{-1}, and its micro- and mesopore volumes were 0.56 and 0.28, respectively. It was found that the proportion of microporosity to total porosity, $V_{DR}/V_{0.99}$, is 0.68, demonstrating that ACFB is mainly microporous with a small portion of mesopores.

The SEM and TEM images of the ACFB sample in figure 3*a*,*b* reveal a great number of the pores (micrometre and nanometre in size), which were formed during the carbonization and activation processes. Pore system and excellent pore morphology observed by SEM and TEM agree with those obtained from BET analysis. Such porosity should definitely provide ACFB with high adsorption capacity towards MB.

The TGA, FTIR, XPS spectra and elemental analysis were carried out to investigate the thermostability and surface properties of ACFB in our previous work [24,35]. Upon heating to high temperature, pyrolysis of organic substances produces volatile products, which means that most of the non-carbon elements, hydrogen, nitrogen and oxygen are removed in gaseous form by pyrolytic decomposition, and leave a solid residue enriched in carbon [35]. The results of XPS spectra and elemental analysis also respond to the conclusion that the obtained AC is pure [24].

3.2. Effect of adsorption process parameters on the removal of MB

3.2.1. Effect of adsorption duration and contact time between MB and ACFB

The contact time is a non-negligible parameter for the MB adsorption process. An appropriate contact time cannot only improve the treatment efficiency but also provide the most cost-effective route. Thus, the effect of contact time of MB adsorption on to ACFB was tested at 30°C with 10 mg of ACFB, 100 ml of 20 mg l^{-1} as initial MB concentration and at pH = 7. Adsorption was allowed to proceed for 180 min to determine the optimum adsorption time (see figure 4 for the results). The results revealed that MB adsorption rate increased rapidly. MB removal continued almost linearly during the initial

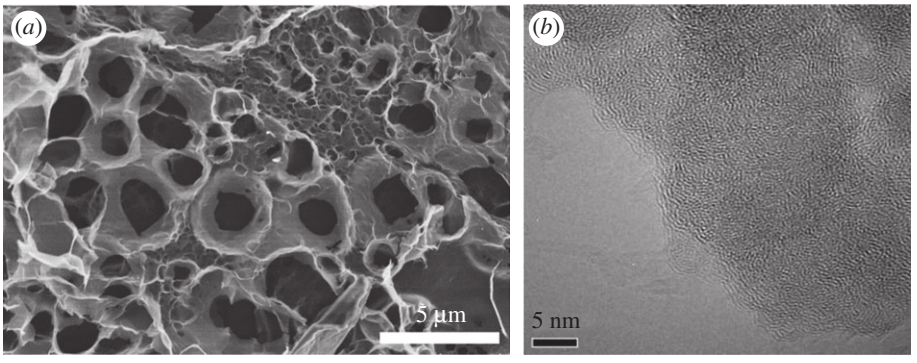

Figure 3. SEM (*a*) and TEM (*b*) images of ACFB.

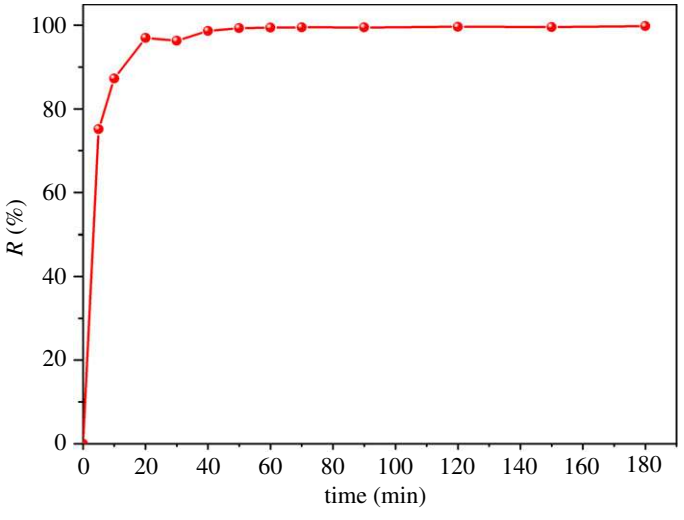

Figure 4. Effect of the contact time on the removal of MB ($C_0 = 20$ mg l^{-1}, $m = 10$ mg, $T = 30$°C, pH = 7, $v = 100$ ml).

contact period, and then gradually slowed down until equilibrium was established at around 20–40 min. Such behaviour was observed because of the higher availability of more active sites on the ACFB surface as well as the weak internal diffusion resistance during early adsorption stages. After the early stages, a plateau formed, during which only an insignificant increase could be seen, mostly because MB content in the solution was significant as active sites were already saturated and diffusion into the ACFB surface pores slowed down [34,38,39].

3.2.2. Effect of activated carbon dosage

The initial amount of an adsorbent is of high significance for adsorption processes. The dosage of the adsorbent at the beginning of the adsorption process affects the total amount of available pores, which will affect the overall adsorption rate and total MB amount adsorbed by ACFB [1,5]. Thus, as initial amounts we used 1, 2.5, 5, 10, 20 and 50 mg of ACFB. All other adsorption parameters were the same: 100 ml of 20 mg l^{-1} MB solution, 30°C, pH = 7 and 180 min equilibration time. Results showing MB removal rates as a function of the initial ACFB content are shown in figure 5. The percentage of removed MB increased dramatically as the weight of the initial ACFB increased: MB removal efficiencies increased from 3.11% at a dosage of 1 mg to 99.78% at a dosage of 10 mg. This can be attributed to the large available surface area as well as abundant active sites for MB molecules to adsorb [40,41].

3.2.3. Effect of the initial concentration of MB on its adsorption

Eight different concentrations (20, 25, 30, 35, 40, 50, 60 and 80 mg l^{-1}) of MB were chosen to study how initial dye MB content affected its adsorption on ACFB. All other experimental adsorption parameters

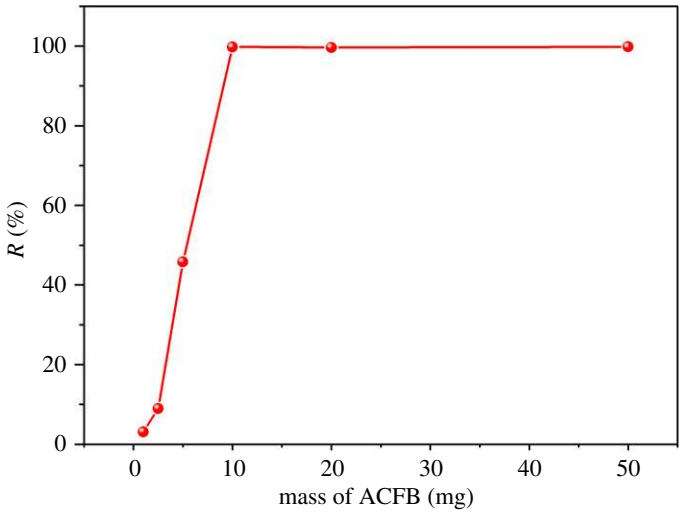

Figure 5. Effect of the AC doses on the removal of MB ($C_0 = 20$ mg l^{-1}, $t = 180$ min, $T = 30$°C, pH = 7, $v = 100$ ml).

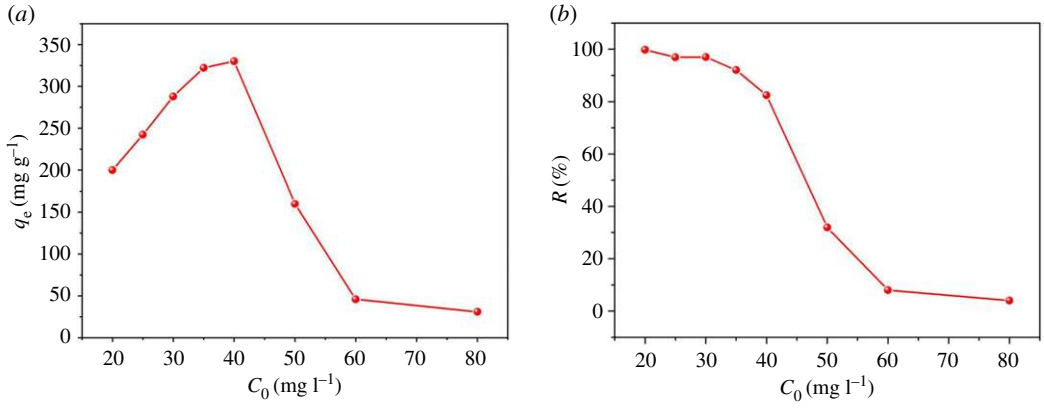

Figure 6. Effect of initial dye concentration of MB on maximum dye uptake (*a*) and the percentage removal by ACFB (*b*) ($m =$ 10 mg, $t = 180$ min, $T = 30$°C, pH = 7, $v = 100$ ml).

were the same: including 100 ml of MB, pH = 7, 10 mg of ACFB, 30°C and 150 rpm agitation speed. As can be seen from figure 6*a*, adsorption curves display two stages of dye uptake as initial MB concentration increases from 20 to 40 mg l^{-1}: the first one demonstrates constantly increasing, and the second one shows decreasing adsorption capacities [42,43]. At a relatively lower dye concentration, higher dye content concentration will increase the effective contact area between dye molecules and ACFB. It will also provide the necessary driving force to overcome MB mass transfer resistance on the interface, which drives adsorption to higher capacity values [16,40]. At MB concentrations above 40 mg l^{-1}, a majority of the active sites are consumed. Therefore, MB adsorption slows down, and a lot of MB in the second phase remains in the solution, which was seen during the second of our adsorption tests [34,44]. Figure 6*b* displays decreased removal constant as initial MB concentration increases. Lower consumption of MB at its higher concentrations was because of high MB/active sites ratio. The ACFB surface quickly becomes saturated with MB at high concentrations, implying the dependence of adsorption on MB initial concentration [42].

3.2.4. pH effect

pH is also considered as one of most essential factors affecting adsorption processes, mostly because it affects adsorbent surface charge. To test how pH affects MB adsorption processes on ACFB, we performed adsorption experiments in the wide pH range and at 20 mg l^{-1} initial MB concentration, 10 mg ACFB dose, at 30°C and 60 min equilibration time. MB removal percentage increased slightly as pH values increased from 3 to 11 (figure 7). At low pH, abundant H^+ compete with MB cations for the active sites. Thus, MB adsorption on ACFB becomes inhibited at low pH vales. Therefore,

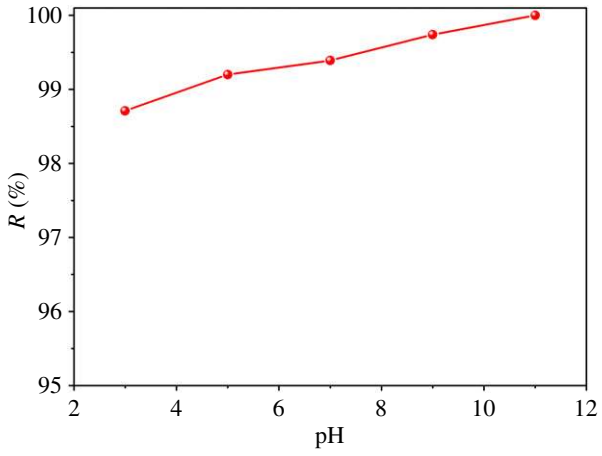

Figure 7. Effect of the pH on the removal of MB ($C_0 = 20$ mg l^{-1}, $m = 10$ mg, $t = 60$ min, $T = 30$°C, $v = 100$ ml).

as mid-level pH values, there are less competitive protons in the solution, which is beneficial for MB adsorption on the ACFB surface [45]. However, our results showed over 98% removal percentage values of MB in both acidic and neutral pH values. This is due to the fact that at low pH, MB remains at cationic and molecular form and can enter into the pores of the adsorbent surface very easily. With increasing pH, the surface of the adsorbent becomes more negative, making it favourable for the cationic dye adsorption [40]. Thus, MB adsorption on ACFB is governed not only by electrostatic interactions but also by van der Waals attraction, π- and other chemical interactions between MB and ACFB surface [38]. In order to get a deep insight in the surface chemical properties of ACFB, the FTIR spectra and XPS analysis were conducted in the previous work [35]. The existence of functional groups such as –COOH, –OH and –NH, on the surface of ACFB, suggests that the carbon material is CxOH, where Cx = carbon. It is necessary to note that the hydroxylated surface groups vary at different pH values because of the protonation/deprotonation processes (i.e. $CxOH + H^+ \leftrightarrow CxOH_2^+$ at low pH, and $CxOH \leftrightarrow CxO^- + H^+$ at high pH) [45].

3.3. Adsorption isotherms

Adsorption isotherms obtained in this work were fitted using the Langmuir, Freundlich and Tempkin models. Their correlation with our adsorption processes was judged by the values of correlation coefficient (R^2) and errors.

The Langmuir model assumes monolayer adsorption on a homogeneous surface with all active sites being equivalent and with the same energy. The Langmuir model also assumes dynamic equilibrium and no interaction between adsorbates [43]. It is typically described by the following formula [46]:

$$\frac{C_e}{q_e} = \frac{C_e}{q_{max}} + \frac{1}{q_{max} K_L}, \tag{3.1}$$

where q_e is the amount of adsorbed dye at the equilibrium (in mg g^{-1}), q_{max} correlates with the maximum monolayer adsorption capacity (in mg g^{-1}), K_L is an adsorption constant describing affinity between MB and ACFB (in l mg^{-1}) and C_e is the MB equilibrium concentration.

The Freundlich model is described by a formula assuming heterogeneous multilayer adsorption on heterogeneous surfaces. The Freundlich model also assumes interactions between the adsorbates and that adsorption capacity increases with the analyte concentration. The formula describing the Freundlich model is shown below [47]

$$\log q_e = \frac{1}{n_F} \log\ C_e + \log\ K_F, \tag{3.2}$$

where K_F is the reaction constant reflecting adsorption capacity (in l mg^{-1}), and $1/n_F$ indicates the dimensionless exponent of the Freundlich model to show adsorption intensity (it is calculated from the slope and an intercept of log q_e versus log C_e plot).

The Temkin adsorption assumes a decrease in adsorption heat because of the adsorbent/adsorbate interaction as coverage with molecular layers increases. Mathematically, it can be expressed as [40,48]

$$q_e = B \ln K_T + B \ln C_e, \tag{3.3}$$

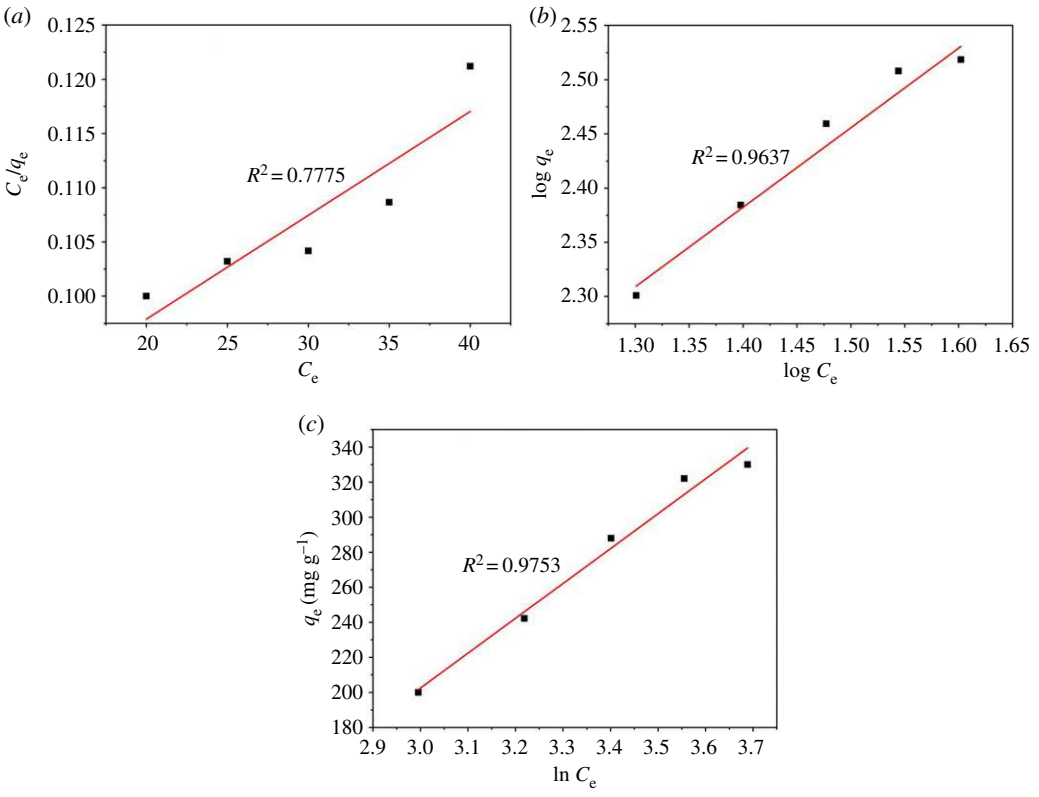

Figure 8. Plots of Langmuir (*a*), Freundlich (*b*) and Temkin (*c*) isotherm models for the adsorption of MB into ACFB.

Table 1. Adsorption isotherm parameters for MB on ACFB.

model								
Langmuir constants			Freundlich constants			Temkin constants		
q_{max}	K_L	R^2	$1/n$	K_F	R^2	B	K_T	R^2
1044.404	0.01216	0.778	0.758	21.086	0.964	199.006	0.138	0.975

where $B = RT/b$, b is the Temkin constant related to the adsorption heat (in J mol^{-1}), K_T (l mg^{-1}) is the equilibrium adsorption constant, R is the gas constant equal to 8.314 J K mol^{-1} and T (K) is the absolute temperature.

Figure 8 displays the Langmuir, Temkin and Freundlich isotherms for our adsorption experiments. The calculated parameters for all these isotherms along with R^2 values are shown in table 1. The correlation coefficient (R^2) for the linear portion of the Temkin model is the closest to 1.0. Thus, the Temkin model describes MB adsorption on ACFB the best. Meanwhile, it reveals this adsorption is not a monolayer adsorption process. The correlation coefficient R^2 for the Freundlich model was above R^2 obtained by fitting the Langmuir model to our data, which very likely indicates that MB adsorption on ACFB does not occur in a monolayer fashion on a homogeneous surface but rather on a heterogeneous one [3]. The value of $1/n$ equal to 0.758 is less than 1, which indicates favourable adsorption conditions [5,6,49].

3.4. Kinetics studies

Adsorption kinetics studies the relationship between adsorption capacity and reaction time. Thus, its main concern is adsorption speed, dynamic equilibrium, mass transfer and diffusion rates. Analysis of these parameters helps to understand adsorption process rates as well as adsorption mechanism.

For adsorption kinetics study, in this work, we used 0.01 g of adsorbent and 100 ml of 20 mg l^{-1} MB solution, and then placed them into a 250 ml beaker at 30°C. We examined the adsorption rate and MB

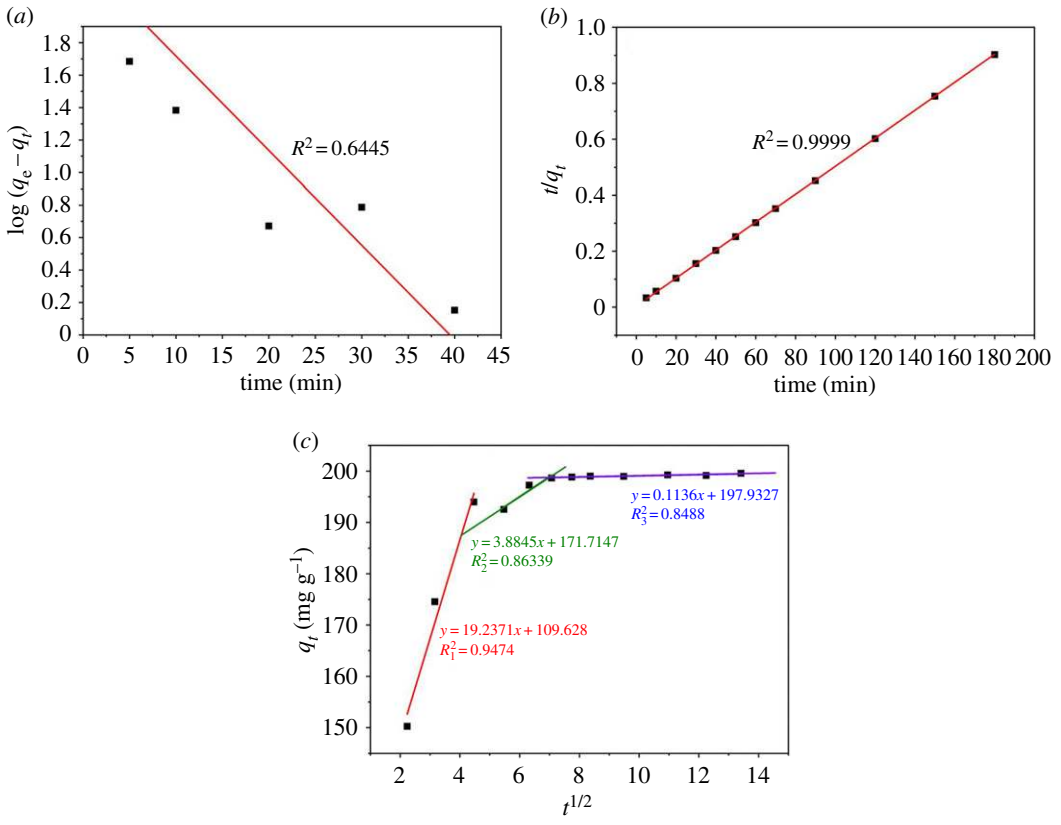

Figure 9. Plots of pseudo-first order (*a*), pseudo-second order (*b*) and intraparticle diffusion (*c*) for the adsorption of MB into ACFB.

removal mechanism by ACFB using different equilibrium times (5–180 min) to understand and develop a solid/liquid-phase equilibrium kinetic model.

Our experimental data were fit using the pseudo-first and -second-order reaction models as well as an intraparticle diffusion model with the goal of establishing adsorption rates.

The pseudo-first-order model is mathematically described as shown below [50]

$$\log(q_e - q_t) = \log q_e - K_1 t, \tag{3.4}$$

where k_1 is the pseudo-first-order kinetic constant (in $1/\text{min}^{-1}$) and t is the time (in min).

The pseudo-second-order kinetic model can be expressed by the following equation [50,51]:

$$\frac{t}{q_t} = \frac{1}{K_2 q_e^2} + \frac{t}{q_e}, \tag{3.5}$$

where k_2 is the pseudo-second-order kinetic constant (in g (mg min)$^{-1}$), q_t correlates with adsorption capacity at time t in minutes (in mg g^{-1}).

Our experimental data were also treated using the intraparticle diffusion model to understand the diffusion process of MB on ACFB particles. It is defined as [50]

$$q_t = K_p t^{1/2} + C, \tag{3.6}$$

where K_p is the intraparticle diffusion constant (in mg g^{-1} min$^{0.5}$) and C is the thickness of the boundary layer. At $C = 0$, intraparticle diffusion is the only controlling step. Thus, adsorption occurs inside the adsorbent. The larger the C, the greater the boundary layer effect on the adsorption, or in other words, the greater the effect of membrane diffusion on the adsorption process.

Figure 9 shows the three models' fitting results. Meanwhile, the detailed parameters calculated from the three kinetic models along with R^2 values are shown in table 2. The correlation coefficient (R^2) of the pseudo-second-order model was higher than the correlation coefficients obtained from other models. Compared to q_e values obtained by fitting our experimental data using the pseudo-first-order and intraparticle diffusion models, the calculated q_e values from the pseudo-second order show better agreement with the experimental values. Thus, taking into account all experimental data mentioned

Table 2. Kinetic model parameters for MB on ACFB.

kinetic models and parameters		MB
pseudo-first-order kinetics	q_e	198.67
	K_1	0.058
	R^2	0.6445
pseudo-second-order kinetics	q_e	199.55
	K_2	0.0071
	R^2	0.9999
intraparticle diffusion	q_e	199.55
	K_p	2.99
	C	169.19
	R_1^2	0.4478
linear fitting intraparticle diffusion	K_{p1}	19.24
	C_1	109.63
	R_1^2	0.9474
	K_{p2}	3.88
	C_2	171.71
	R_2^2	0.8634
	K_{p3}	0.11
	C_3	197.93
	R_3^2	0.8488

above, we determined that the pseudo-second-order kinetic model agrees the best with MB adsorption on ACFB than other kinetic models.

Figure 9*c* displays our experimental results fitted using the intraparticle diffusion model. The *C*-value was not zero. All corresponding curves are multilinear, and three main adsorption stages can be clearly distinguished. The initial stage with slope K_{p1} (19.24) shows that the dye molecules are adsorbed from the liquid phase to the external adsorbent surfaces. The second stage had K_{p2} equal to 3.88, which reveals that dye molecules enter ACFB internal pores from its surface. Such a phenomenon is called intraparticle diffusion. The third stage with the K_{p3} equal to 0.11 represents MB adsorption on the ACFB sites. During these stages, as MB concentration in the solution decreased, mass transfer resistance of the adsorbate increased. As a result, the diffusion process gradually slowed down, and the slope became less steep [2,14,40,52].

Table 3 shows the adsorption capacities of ACs prepared from other agricultural by-products, polymers and carbon composite materials. It is clear from these data that AC is one of the lowest cost and one of the most effective adsorbents for MB and other organics removal. What is more, as mentioned, FB is a sort of common forestry waste, which means that the cost of FB is lower than the normal biomass, polymers or GO for AC production, such as bamboo, wood, rice husk, coconut shell, graphene and so on. All these merits, along with the zero-cost and wide availability of FB, make this type of sorbent highly promising in dye adsorption.

3.5. Regeneration of adsorbent

According to the above analysis, MB can be easily adsorbed into ACFB under moderate conditions. In order to get further into the practical application, the regeneration property was investigated using ethanol as the eluent. As shown in figure 10, the removal capacity of MB retained 69.41% after four cycles, indicating the ACFB material possesses good regenerability and reusability when using ethanol solution [61–63].

3.6. Adsorption mechanism

The MB can be better removed by AC under both acid and basic conditions, indicating that the electrostatic interaction played an important role in the adsorption process [63]. At lower pH, the

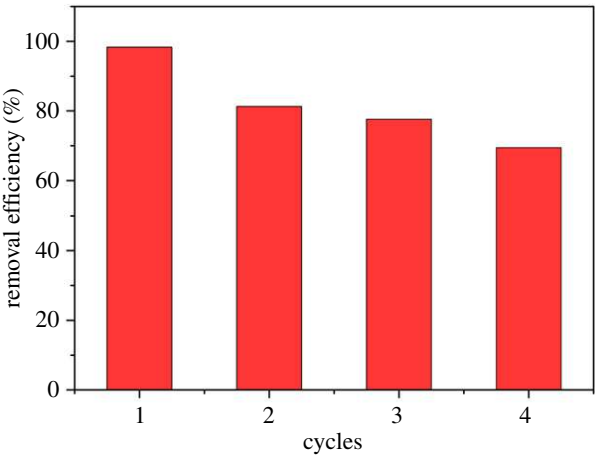

Figure 10. Regeneration of ACFB and MB desorption.

Table 3. Comparison of adsorption capacity of various adsorbents for MB.

adsorbent	q_e (mg g^{-1})	ref.
fir bark activated carbon	330	this work
banana trunk activated carbon	166	[53]
Acacia mangium wood activated carbon	158	[51]
cork powder waste activated carbon	350	[52]
date pits activated carbon	259	[6]
Filtrasorb 400,	255	[54]
Norit and	222	
Picacarb granular activated carbon	160	
cotton stalk	147	[55]
CuS nanoparticle loaded on activated carbon	208	[56]
Ephedra strobilacea saw dust char	31	[57]
GO	302	[58]
graphene oxide/cellulose	375	[59]
graphene oxide/titanate nanotube	26	[19]
chitosan	385	[60]
graphite oxide	170	[20]

various functional groups and reactive atom of dyes and adsorbent protonated and both get positive charge [40]. At higher pH, the carboxylic groups are deprotonated, and negatively charged carboxylate ligands (COO–) bind to the positively charged MB molecules. This finding confirms that the sorption of MB by FBAC is an ion exchange mechanism between the negatively and the positively charged groups [41,64]. Therefore, due to the strong repulsive force between dye and adsorbent the removal percentage decreased. The results of equilibrium and kinetic studies showed that the adsorption of MB onto FBAC was predominantly a chemisorption process [45]. Therefore, electrostatic interaction along with chemical binding between adsorbate and adsorbent mainly controlled the MB/FBAC adsorption process.

4. Conclusion

ACFB was prepared. It demonstrated substantial adsorption relative to MB because of its very high surface area (approx. 1552 $m^2 g^{-1}$) and large pore volume (approx. 0.84 $cm^3 g^{-1}$). The maximum MB

adsorption capacity of ACFB was 330 mg g^{-1}. In general, the adsorption capacity of ACFB relative to MB increased with longer equilibrium times, higher adsorbent dosage and higher initial MB concentrations. Adsorption data can be fit with a good correlation coefficient using the Freundlich and Temkin models. Adsorption kinetics followed the pseudo-second-order model. Overall, ACFB demonstrated outstanding adsorption properties relative to MB and cationic dyes in general. Thus, ACFB is very promising for use in wastewater treatment to mitigate dye pollution.

Data accessibility. The data that support the findings of this study are openly available from the Dryad Digital Repository: https://doi.org/10.5061/dryad.8tn1qg5 [65].

Authors' contributions. W.Z. and M.F. designed this work; L.L., X.W., T.C. and Z.L. performed the experiments; W.Z., L.L., Y.Z. and Z L. analysed the data; W.Z. and L.L. wrote this paper. All authors gave final approval for publication.

Competing interests. We have no competing interests.

Funding. Financial support came from the Natural Science Foundation of Fujian Province Department of Science and Technology, grant no. 2019J01386; Forestry science and technology research project of Fujian Forestry Department of China, grant no. KLB18H02A; National Natural Science Foundation of China, grant no. 31971593; Fujian Agriculture and Forestry University Fund for Distinguished Young Scholars, grant no. xjq201420.

Acknowledgements. We gratefully acknowledge the anonymous reviewers for their constructive comments which have improved the quality of this paper.

References

1. Maneerung T, Liew J, Dai Y, Kawi S, Chong C, Wang C. 2015 Activated carbon derived from carbon residue from biomass gasification and its application for dye adsorption: kinetics, isotherms and thermodynamic studies. *Bioresour. Technol.* **200**, 350–359. (doi:10.1016/j.biortech.2015.10.047)
2. Angin D. 2014 Utilization of activated carbon produced from fruit juice industry solid waste for the adsorption of Yellow 18 from aqueous solutions. *Bioresour. Technol.* **168**, 259–266. (doi:10.1016/j.biortech.2014.02.100)
3. Zhang W, Li H, Kan X, Dong L, Yan H, Jiang Z, Yang H, Li A, Cheng R. 2012 Adsorption of anionic dyes from aqueous solutions using chemically modified straw. *Bioresour. Technol.* **117**, 40–47. (doi:10.1016/j.biortech.2012.04.064)
4. Gerçel Ö, Özcan A, Özcan AS, Ferdi GH. 2007 Preparation of activated carbon from a renewable bio-plant of *Euphorbia rigida* by H_2SO_4 activation and its adsorption behavior in aqueous solutions. *Appl. Surf. Sci.* **253**, 4843–4852. (doi:10.1016/j.apsusc.2006.10.053)
5. Kazeem TS, Lateef SA, Ganiyu SA, Qamaruddin M, Tanimu A, Sulaiman KO, Jillani SMS, Alhooshani K. 2018 Aluminium-modified activated carbon as efficient adsorbent for cleaning of cationic dye in wastewater. *J. Clean. Prod.* **205**, 303–312. (doi:10.1016/j.jclepro.2018.09.114)
6. Theydan SK, Ahmed MJ. 2012 Adsorption of methylene blue onto biomass-based activated carbon by $FeCl_3$ activation: equilibrium, kinetics, and thermodynamic studies. *J. Anal. Appl. Pyrol.* **97**, 116–122. (doi:10.1016/j.jaap.2012.05.008)
7. Rubio J, Souza ML, Smith RW. 2002 Overview of flotation as a wastewater treatment technique. *Miner. Eng.* **15**, 139–155. (doi:10.1016/S0892-6875(01)00216-3)
8. Seshadri S, Bishop PL, Agha AM. 1994 Anaerobic/aerobic treatment of selected Azo dyes in wastewater. *Waste Manage.* **14**, 127–137. (doi:10.1016/0956-053X(94)90005-1)
9. Choo KH, Chang DI, Park KW, Kim MH. 2008 Use of an integrated photocatalysis/hollow fiber microfiltration system for the removal of trichloroethylene in water. *J. Hazard. Mater.* **152**, 183–190. (doi:10.1016/j.jhazmat.2007.06.117)
10. Wu JS, Liu CH, Chu KH, Suen SY. 2008 Removal of cationic dye Methyl violet 2B from water by cation exchange membranes. *J. Membr. Sci.* **309**, 239–245. (doi:10.1016/j.memsci.2007.10.035)
11. Chen J, Wang Y, Liu Y, Tang M, Wang R, Tian Y, Jia C. 2019 Bacterial community shift and antibiotics resistant genes analysis in response to biodegradation of oxytetracycline in dual graphene modified bioelectrode microbial fuel cell. *Bioresour. Technol.* **276**, 236–243. (doi:10.1016/j.biortech.2019.01.006)
12. Karthikeyan S, Gupta VK, Boopathy R, Titus A, Sekaran G. 2012 A new approach for the degradation of high concentration of aromatic amine by heterocatalytic fenton oxidation: kinetic and spectroscopic studies. *J. Mol. Liq.* **173**, 153–163. (doi:10.1016/j.molliq.2012.06.022)
13. Chen J, Yang Y, Liu Y, Tang M, Wang R, Zhang C, Jiang J, Jia C. 2019 Bacterial community shift in response to a deep municipal tail wastewater treatment system. *Bioresour. Technol.* **281**, 195–201. (doi:10.1016/j.biortech.2019.02.099)
14. Wang X, Jiang C, Hou B, Wang Y, Hao C, Wu J. 2018 Carbon composite lignin-based adsorbents for the adsorption of dyes. *Chemosphere* **206**, 587–596. (doi:10.1016/j.chemosphere.2018.04.183)
15. Ait Ahsaine H, Zbair M, Anfar Z, Naciri Y, El Haouti R, El Alem N, Ezahri M. 2018 Cationic dyes adsorption onto high surface area 'almond shell' activated carbon: kinetics, equilibrium isotherms and surface statistical modelling. *Mater. Today Chem.* **8**, 121–132. (doi:10.1016/j.mtchem.2018.03.004)
16. Enniya I, Rghioui L, Jourani A. 2018 Adsorption of hexavalent chromium in aqueous solution on activated carbon prepared from apple peels. *Sustain. Chem. Pharm.* **7**, 9–16. (doi:10.1016/j.scp.2017.11.003)
17. Benkaddour S, Slimani R, Hiyane H, El Ouahabi I, Hachoumi I, El Antri S, Lazar S. 2018 Removal of reactive yellow 145 by adsorption onto treated watermelon seeds: kinetic and isotherm studies. *Sustain. Chem. Pharm.* **10**, 16–21. (doi:10.1016/j.scp.2018.08.003)
18. Fuat G. 2015 Conversion of grape industrial processing waste to activated carbon sorbent and its performance in cationic and anionic dyes adsorption. *J. Clean. Prod.* **93**, 84–93. (doi:10.1016/j.jclepro.2015.01.009)
19. Nguyyen CH, Juang R. 2019 Efficient removal of methylene blue dye by a hybrid adsorption–photocatalysis process using reduced graphene oxide/titanatenanotube composites for water reuse. *J. Ind. End. Chem.* **76**, 296–309. (doi:10.1016/j.jiec.2019.03.054)
20. Yang B, Guo Y, Zhang S, Wen T, Zhao C. 2014 Synthesis of graphene by microwave irradiation for dye adsorption. *RSC Adv.* **4**, 64 771–64 780. (doi:10.1039/c4ra12589d)
21. Dehghani M, Dehghani A, Alidadi H, Dolatabadi M, Mehrabpour M, Converti A. 2017 Removal of methylene blue dye from aqueous solutions by a new chitosan/zeolite composite from shrimp waste: kinetic and equilibrium study. *Korean J. Chem. Eng.* **34**, 1699–1707. (doi:10.1007/s11814-017-0077-2)
22. Fu J, Chen Z, Wang M, Liu S, Zhang JG, Zhang J, Han R, Xu Q. 2015 Adsorption of methylene blue by a high-efficiency adsorbent (polydopamine microspheres): kinetics, isotherm, thermodynamics and mechanism analysis. *Chem. Eng. J.* **259**, 53–61. (doi:10.1016/j.cej.2014.07.101)
23. Auta M, Hameed BH. 2014 Chitosan–clay composite as highly effective and low-cost adsorbent for batch and fixed-bed adsorption of methylene blue. *Chem. Eng. J.* **237**, 352–361. (doi:10.1016/j.cej.2013.09.066)
24. Zhao W, Luo L, Wu X, Chen T, Li L, Zhang Z, Rao J, Fan M. 2019 Facile and low-cost

heteroatom-doped activated biocarbons derived from fir bark for electrochemical capacitors. *Wood Sci. Technol*. **53**, 227–248. (doi:10.1007/s00226-018-1065-3)

25. Sayğılı H, Güzel F. 2016 High surface area mesoporous activated carbon from tomato processing solid waste by zinc chloride activation: process optimization, characterization and dyes adsorption. *J. Clean. Prod.* **113**, 995–1004. (doi:10.1016/j.jclepro.2015.12.055)
26. Skouteris G, Saroj D, Melidis P, Hai FI, Ouki S. 2015 The effect of activated carbon addition on membrane bioreactor processes for wastewater treatment and reclamation—a critical review. *Bioresour. Technol.* **185**, 399–410. (doi:10.1016/j.biortech.2015.03.010)
27. Okman I, Selhan K, Tay T, Erdem M. 2014 Activated carbons from grape seeds by chemical activation with potassium carbonate and potassium hydroxide. *Appl. Surf. Sci.* **293**, 138–142. (doi:10.1016/j.apsusc.2013.12.117)
28. Zhao W, Luo Lu, Wang H, Fan M. 2017 Synthesis of bamboo-based activated carbons with super-high specific surface area for hydrogen storage. *Bioresources* **12**, 1246–1262. (doi:10.15376/biores.12.1.1246-1262)
29. Zhao W, Luo L, Chen T, Li Z, Zhang Z, Fan M. 2018 Activated carbons from oil palm shell for hydrogen storage. *Mater. Sci. Eng.* **368**, 012031. (doi:10.1088/1757-899X/368/1/012031)
30. Aljebori AM, Alshirifi AN, Alkaim AF. 2017 Kinetics and equilibrium study for the adsorption of textile dyes on coconut shell activated carbon. *Arab. J. Chem.* **10**, S3381–S3393. (doi:10.1016/j.arabjc.2014.01.020)
31. Singh G, Kim IY, Lakhi KS, Srivastava P, Naidu R, Vinu A. 2017 Single step synthesis of activated bio-carbons with a high surface area and their excellent CO_2 adsorption capacity. *Carbon* **116**, 448–455. (doi:10.1016/j.carbon.2017.02.015)
32. Li W, Ma T, Zhang R, Tian Y, Qiao Y. 2015 Preparation of porous carbons with high low-pressure CO_2 uptake by KOH activation of rice husk char. *Fuel* **139**, 68–70. (doi:10.1016/j.fuel.2014.08.027)
33. Zhu X, Wang P, Peng C, Yang J, Yan X. 2014 Activated carbon produced from paulownia sawdust for high-performance CO_2 sorbents. *Chin. Chem. Lett.* **25**, 929–932. (doi:10.1016/j.cclet.2014.03.039)
34. Djilani C, Zaghdoudi R, Djazi F, Bouchekima B, Lallam A, Modarressi A, Rogalski M. 2015 Adsorption of dyes on activated carbon prepared from apricot stones and commercial activated carbon. *J. Taiwan Ins. Chem. E* **53**, 112–121. (doi:10.1016/j.jtice.2015.02.025)
35. Luo L, Chen T, Li Z, Zhang Z, Zhao W, Fan M. 2018 Heteroatom self-doped activated biocarbons from fir bark and their excellent performance for carbon dioxide adsorption. *J. CO_2 Util.* **25**, 89–98. (doi:10.1016/j.jcou.2018.03.014)
36. Silva TL, Cazetta AL, Souza PSC, Zhang T, Asefa T, Almeida VC. 2017 Mesoporous activated carbon fibers synthesized from denim fabric waste: efficient adsorbents for removal of textile dye from aqueous solutions. *J. Clean. Prod.* **171**, 482–490. (doi:10.1016/j.jclepro.2017.10.034)
37. Thommes M, Kaneko K, Neimark AV, Olivier JP, Rodriguez-Reinoso F, Rouquerol J, Rodriguez-Reinoso F, Rouquerol J, Sing KSW. 2015 Physisorption of gases, with special reference to the evaluation of surface area and pore size distribution (IUPAC Technical Report). *Pure Appl. Chem.* **38**, 25. (doi:10.1515/pac-2014-1117)
38. Heidarinejad Z, Rahmanian O, Fazlzadeh M, Heidari M. 2018 Enhancement of methylene blue adsorption onto activated carbon prepared from date press cake by low frequency ultrasound. *J. Mol. Liq.* **264**, 591–599. (doi:10.1016/j.molliq.2018.05.100)
39. Priyanka M, Saravanakumar MP. 2018 Ultrahigh adsorption capacity of starch derived zinc based carbon foam for adsorption of toxic dyes and its preliminary investigation on oil-water separation. *J. Clean. Prod.* **197**, 511–524. (doi:10.1016/j.jclepro.2018.06.197)
40. Goswami M, Phukan P. 2017 Enhanced adsorption of cationic dyes using sulfonic acid modified activated carbon. *J. Environ. Chem. Eng.* **5**, 3508–3517. (doi:10.1016/j.jece.2017.07.016)
41. Bouaziz F, Koubaa M, Kallel F, Ghorbel RE, Chaabouni SE. 2017 Adsorptive removal of malachite green from aqueous solutions by almond gum: kinetic study and equilibrium isotherms. *Int. J. Biol. Macromol.* **105**, 56–65. (doi:10.1016/j.ijbiomac.2017.06.106)
42. Azouaou N, Sadaoui Z, Djaafri A, Mokaddem H. 2010 Adsorption of cadmium from aqueous solution onto untreated coffee grounds: equilibrium, kinetics and thermodynamics. *J. Hazard. Mater.* **184**, 126–134. (doi:10.1016/j.jhazmat.2010.08.014)
43. Sangon S, Hunt AJ, Attard TM, Mengchang P, Supanchaiyamat N. 2017 Valorisation of waste rice straw for the production of highly effective carbon based adsorbents for dyes removal. *J. Clean. Prod.* **172**, 1128–1139. (doi:10.1016/j.jclepro.2017.10.210)
44. Rao MM, Rao GPC, Seshaiah K, Choudary NV, Wang MC. 2008 Activated carbon from ceiba pentandra hulls, an agricultural waste, as an adsorbent in the removal of lead and zinc from aqueous solutions. *Waste Manage.* **28**, 849–858. (doi:10.1016/j.wasman.2007.01.017)
45. Hu J, Chen C, Zhu X, Wang X. 2009 Removal of chromium from aqueous solution by using oxidized multiwalled carbon nanotubes. *J. Hazard. Mater.* **162**, 1542–1550. (doi:10.1016/j.jhazmat.2008.06.058)
46. Langmuir I. 1916 The constitution and fundamental properties of solids and liquids. *J. Am. Chem. Soc.* **38**, 2221–2295. (doi:10.1016/s0016-0032(17)90938-x)
47. Ghaedi M, Nasab AG, Khodadoust S, Rajabi M, Azizian S. 2014 Application of activated carbon as adsorbents for efficient removal of methylene blue: kinetics and equilibrium study. *J. Ind. Eng. Chem.* **20**, 2317–2324. (doi:10.1016/j.jiec.2013.10.007)
48. Temkin MJ, Pyzhev V. 1940 Recent modifications to Langmuir isotherms. *Acta Phys.* **12**, 217–222.
49. Namasivayam C, Jeyakumar R, Yamuna RT. 1994 Dye removal from wastewater by adsorption on 'waste' fe(III)/cr(III) hydroxide. *Waste Manage.* **14**, 643–648. (doi:10.1016/0956-053X(94)90036-1)
50. Low KS, Lee CK, Tan KK. 1995 Biosorption of basic dyes by water hyacinth roots. *Bioresour. Technol.* **52**, 79–83. (doi:10.1016/0960-8524(95)00007-2)
51. Ho YS. 2006 Review of second-order models for adsorption systems. *J. Cheminform.* **136**, 681–689. (doi:10.1016/j.jhazmat.2005.12.043)
52. Wong S, Yac'Cob NAN, Ngadi N, Hassan O, Inuwa IM. 2018 From pollutant to solution of wastewater pollution: synthesis of activated carbon from textile sludge for dye adsorption. *Chin. J. Chem. Eng.* **26**, 870–878. (doi:10.1016/j.cjche.2017.07.015)
53. Ho YS, Mckay G. 1999 Pseudo-second order model for sorption processes. *Process Biochem.* **34**, 451–465. (doi:10.1016/S0032-9592(98)00112-5)
54. Mohammed D, Tanweer A, Shahnaz M, Mehraj A, Lou Z, Zhou P, Shakeel ISM. 2018 Use of banana trunk waste as activated carbon in scavenging methylene blue dye: kinetic, thermodynamic, and isotherm studies. *Bioresour. Technol.* **3**, 127–137. (doi:10.1016/j.biteb.2018.07.007)
55. Danish M, Ahmad T, Hashim R, Said N, Akhtar MN, Mohamad-Saleh J, Sulaiman O. 2018 Comparison of surface properties of wood biomass activated carbons and their application against rhodamine B and methylene blue dye. *Surf. Interface* **11**, 1–13. (doi:10.1016/j.surfin.2018.02.001)
56. Novais RM, Caetano APF, Seabra MP, Labrincha JA, Pullar RC. 2018 Extremely fast and efficient methylene blue adsorption using eco-friendly cork and paper waste-based activated carbon adsorbents. *J. Clean. Prod.* **197**, 1137–1147. (doi:10.1016/j.jclepro.2018.06.278)
57. Raposo F, Rubia MADL, Borja R. 2009 Methylene blue number as useful indicator to evaluate the adsorptive capacity of granular activated carbon in batch mode: influence of adsorbate/adsorbent mass ratio and particle size. *J. Hazard. Mater.* **165**, 291–299. (doi:10.1016/j.jhazmat.2008.09.106)
58. Deng H, Lu J, Li G, Zhang G, Wang X. 2011 Adsorption of methylene blue on adsorbent materials produced from cotton stalk. *Chem. Eng. J.* **172**, 326–334. (doi:10.1016/j.cej.2011.06.013)
59. Mazaheri H, Ghaedi M, Asfaram A, Hajati S. 2016 Performance of Cus nanoparticle loaded on activated carbon in the adsorption of methylene blue and bromophenol blue dyes in binary aqueous solutions: using ultrasound power and optimization by central composite design. *J. Mol. Liq.* **219**, 667–676. (doi:10.1016/j.molliq.2016.03.050)
60. Agarwal S, Tyagi I, Gupta VK, Ghasemi N, Shahivand M, Ghasemi M. 2016 Kinetics, equilibrium studies and thermodynamics of methylene blue adsorption on *Ephedra strobilacea* saw dust and modified using phosphoric acid and zinc chloride. *J. Mol. Liq.* **218**, 208–218. (doi:10.1016/j.molliq.2016.02.073)
61. Ramezani S, Zahedi P, Bahrami S, Nemati Y. 2019 Microfluidic fabrication of nanoparticles

based on ethyl acrylate-functionalized chitosan for adsorption of methylene blue from aqueous solutions. *J. Polym. Environ.* **27**, 1653–1665. (doi:10.1007/s10924-019-01463-6)

62. Hussain I, Li Y, Qi J, Li J, Wang L. 2018 Nitrogen-enriched carbon sheet for Methyl blue dye adsorption. *J. Environ. Manage.* **215**, 123–131. (doi:10.1016/j.jenvman.2018.03.051)
63. Regti A, Laamari M, Stiriba S, Haddad M. 2017 Potential use of activated carbon derived from Persea species under alkaline conditions for removing cationic dye from wastewaters. *J. Assoc. Arab Univers. Basic Appl. Sci.* **24**, 10–18. (doi:10.1016/j.jaubas.2017.01.003)
64. Saeed A, Sharif M, Iqbal M. 2010 Application potential of grapefruit peel as dye sorbent: kinetics, equilibrium and mechanism of crystal violet adsorption. *J. Hazard. Mater.* **179**, 564–572. (doi:10.1016/j.jhazmat.2010.03.041)
65. Luo L, Wu X, Li Z, Zhou Y, Chen T, Fan M, Zhao W. 2019 Data from: Synthesis of activated carbon from biowaste of fir bark for methylene blue removal. Dryad Digital Repository. (doi:10.5061/dryad.8tn1qg5)